Kempka, T., Nielsen, C. M., Frykman, P., Shi, J.-Q., Bacci, G., Dalhoff, F. (2015): Coupled Hydro-Mechanical Simulations of CO2 Storage Supported by Pressure Management Demonstrate Synergy Benefits from Simultaneous Formation Fluid Extraction. - *Oil & Gas Science and Technology*, *70*, 4, pp. 599—613.

DOI: http://doi.org/10.2516/ogst/2014029

Oil & Gas Science and Technology – Rev. IFP Energies nouvelles

DOI: 10.2516/ogst/2014029

Dossier

Characterization of European CO_2 Storage – European Project SiteChar
Charactérisation de sites européens de stockage de CO_2 – Projet européen SiteChar

Coupled Hydro-Mechanical Simulations of CO_2 Storage Supported by Pressure Management Demonstrate Synergy Benefits from Simultaneous Formation Fluid Extraction

Thomas Kempka[1]*, Carsten Møller Nielsen[2], Peter Frykman[2], Ji-Quan Shi[3], Giacoma Bacci[3] and Finn Dalhoff[4]

[1] *GFZ German Research Centre for Geosciences, Telegrafenberg, 14473 Potsdam - Germany*
[2] *Geological Survey of Denmark and Greenland (GEUS), Øster Voldgade 10, 1350 Copenhagen - Denmark*
[3] *Imperial College London (ICL), South Kensington Campus, London SW7 2AZ - UK*
[4] *Vattenfall R&D, Støberigade 14, 2450 Copenhagen SV - Denmark*
e-mail: kempka@gfz-potsdam.de

* Corresponding author

Abstract — *We assessed the synergetic benefits of simultaneous formation fluid extraction during CO_2 injection for reservoir pressure management by coupled hydro-mechanical simulations at the prospective Vedsted storage site located in northern Denmark. Effectiveness of reservoir pressure management was investigated by simulation of CO_2 storage without any fluid extraction as well as with 66% and 100% equivalent volume formation fluid extraction from four wells positioned for geothermal heat recovery. Simulation results demonstrate that a total pressure reduction of up to about 1.1 MPa can be achieved at the injection well. Furthermore, the areal pressure perturbation in the storage reservoir can be significantly decreased compared to the simulation scenario without any formation fluid extraction. Following a stress regime analysis, two stress regimes were considered in the coupled hydro-mechanical simulations indicating that the maximum ground surface uplift is about 0.24 m in the absence of any reservoir pressure management. However, a ground uplift mitigation of up to 37.3% (from 0.24 m to 0.15 m) can be achieved at the injection well by 100% equivalent volume formation fluid extraction. Well-based adaptation of fluid extraction rates can support achieving zero displacements at the proposed formation fluid extraction wells located close to urban infrastructure. Since shear and tensile failure do not occur under both stress regimes for all investigated scenarios, it is concluded that a safe operation of CO_2 injection with simultaneous formation fluid extraction for geothermal heat recovery can be implemented at the Vedsted site.*

Résumé — **Des simulations du comportement hydromécanique d'un réservoir géologique de stockage de CO_2 dans un contexte de gestion de la pression démontrent les avantages de l'extraction de fluide de la formation au cours de l'injection du CO_2** — Au moyen de simulations hydromécaniques couplées menées sur le site de stockage prospectif Vedsted situé au nord du Danemark, nous avons évalué les avantages de l'extraction du fluide de la formation au cours de l'injection de CO_2 dans un but de gestion de la pression dans le réservoir. L'efficacité de la gestion de la

pression du réservoir a été étudiée par comparaison des simulations du stockage de CO_2 sans extraction de fluide avec celles associées à une extraction d'un volume équivalent de fluide de la formation de 66 % et 100 % à partir de quatre puits dédiés à la récupération géothermique de chaleur. Les résultats des simulations montrent qu'une réduction de la pression totale d'environ 1,1 MPa peut être obtenue au puits d'injection. En outre, la perturbation de pression locale dans le réservoir de stockage peut être nettement diminuée par rapport au scénario de simulation sans extraction de fluide de formation. Après analyse, deux régimes de contrainte ont été considérés dans les simulations hydromécaniques couplées indiquant que l'élévation maximale de la surface au sol est d'environ 0,24 m en l'absence de toute gestion de la pression du réservoir. Toutefois, une atténuation de cette élévation de l'ordre de 37,3 % (de 0,24 m à 0,15 m) peut être obtenue au puits d'injection par extraction d'un volume équivalent du fluide de la formation de 100 %. Une adaptation des taux d'extraction de fluide pourrait permettre une élévation nulle aux puits d'extraction de fluide de formation qui sont par ailleurs situés près d'une infrastructure urbaine. Puisqu'aucune rupture au cisaillement et à la traction n'a été observée pour les deux régimes de contraintes dans tous les scénarios étudiés, nous en concluons que l'injection de CO_2 avec extraction de fluide de la formation en vue de la récupération de chaleur géothermique peut être mise en œuvre de façon sécurisée sur le site de Vedsted.

INTRODUCTION

Different authors (Bergmo *et al.*, 2011; Buscheck *et al.*, 2012; Court *et al.*, 2012; Tillner *et al.*, 2013a; Nielsen *et al.*, 2013) demonstrated that formation fluid extraction supports geological CO_2 storage by increasing storage efficiency and reducing reservoir pressure elevation. Depending on the target formation depth, extracted fluids may be used for geothermal heat recovery or disposed according to national environmental regulations. An active reservoir management by means of formation fluid extraction is required, if CO_2 injection is likely to result in compromising the integrity of the storage formation, caprock or adjacent faults. In case of fluid injection into a reservoir, pore pressure is generally increasing, and thus effective stresses are lowered, while fluid extraction generally decreases pore pressures and increases effective stresses. The interaction of producing saline formation fluids during CO_2 injection into a saline aquifer was yet not assessed by coupled hydro-mechanical simulations. Consequently, we carried out an integrated assessment of the benefits from the hydro-mechanical point of view in the present study. Thereto, numerical dynamic flow simulations carried out by Nielsen *et al.* (2013) were extended by additional simulation scenarios and coupled hydro-mechanical simulations to evaluate potential geomechanical benefits from reservoir management by applying different CO_2 injection and brine extraction scenarios. For that purpose, we investigated vertical displacements at the reservoir top and ground surface as well as potential impacts of the reservoir operation on storage formation, caprock and fault integrity as carried out for single injection and production operations by Vidal-Gilbert *et al.* (2009), Magri *et al.* (2013) and Röhmann *et al.* (2013).

1 STUDY AREA

The study area is the Vedsted site, an anticlinal structural closure, in northern Denmark (about 25 km east of the city of Aalborg) located in the Fjerritslev Trough as a subbasin in the Sorgenfrei-Tornquist Zone (Nielsen, 2003). The main storage reservoir is represented by the regional Upper Triassic – Lower Jurassic Gassum Sand Formation (Dalhoff *et al.*, 2011). Secondary storage potential may be present in the Middle Triassic Haldager Sand Formation which is overlying the Gassum Formation in the study area (*Fig. 1*). The Gassum Formation is about 250 m thick in the Vedsted area and contains two sandy intervals divided by an about 75 m thick interval of marine shales of the Fjerritslev Formation. This shale unit contains different sandstone layers of low thickness and is overlain by marine sandstones of 5 m thickness. The lower 140 m of the Gassum Formation is interpreted as fluvial sandstone interbedded with lacustrine mudstones upward grading into shallow marine sandstones interbedded with marine mudstones, while the upper 50 m of the formation are interpreted as marine shoreface sand (Nielsen, 2003). Available well information indicates a net to gross ratio of 0.74 and a sandstone porosity up to 20% is estimated from core

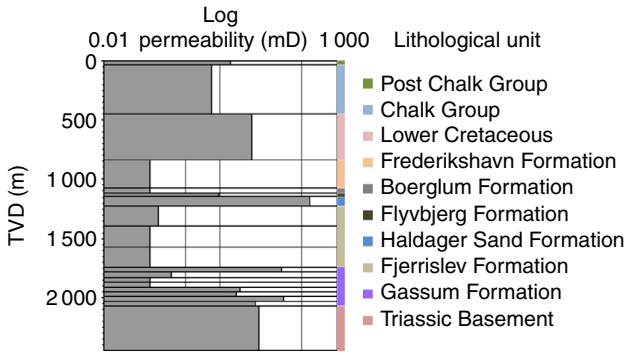

Figure 1

Structural setting determined from Vedsted-1 well data including permeabilities (milli-Darcy) derived from core sample testing and applied in the reservoir simulations.

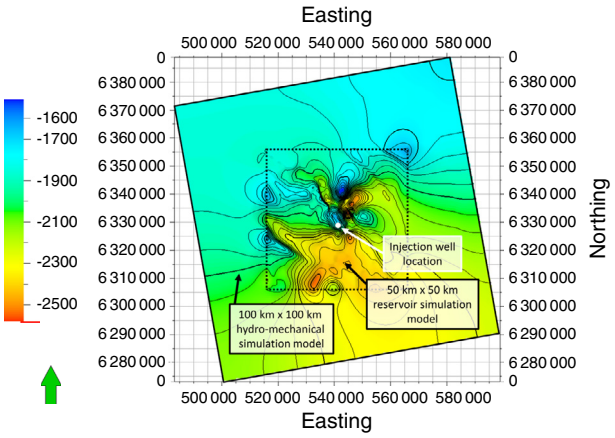

Figure 2

Regional view of elevation depth (m TVD) of the Gassum Formation top and the Vedsted site (figure centre). The size of the reservoir simulation and hydro-mechanical models is indicated by the dashed (50 km × 50 km) and solid (100 km × 100 km) lines, respectively (green arrow points into North direction).

material (Dalhoff *et al.*, 2011; Larsen *et al.*, 2003). Existing oil exploration wells from the 1950s (Vedsted-1 and Haldager-1), top Gassum Formation map (Britze and Japsen, 1991) and available 2D seismic data allowed Frykman *et al.* (2011) to implement a 3D regional structural geological model that was laterally extended and applied as a basis for all simulations in the present study (*Fig. 2*, 3).

The primary caprock of the main storage reservoir (Gassum Formation) is the regional marine mudstone of the Fjerritslev Formation with a 525 m thickness at the Vedsted-1 well location (*Fig. 1*). The Flyvbjerg Formation is the seal of the second reservoir (Haldager Formation), with a thickness of 25 m to 50 m consisting of marine mudstones with intercalated siltstones and sandstones. This formation is followed by a thick succession of about 780 m of mainly marine mudstones of the Borglum, Frederikshavn and Vedsted Formations. The top of the model is represented by the Chalk Group of 400 m thickness and the Post Chalk Group of relatively low thickness (Dalhoff *et al.*, 2011; Larsen *et al.*, 2003).

2 DYNAMIC FLOW SIMULATIONS

Dynamic fluid flow simulations studies were carried out for the Vedsted site by Frykman *et al.* (2009, 2011) and Klinkby *et al.* (2011) to assess CO_2 storage potentials and pressure perturbation in the two main reservoirs. According to Dalhoff *et al.* (2011), the total CO_2 storage potential was estimated to about 160 Mt considering a sweep efficiency of 40%. The dynamic simulation results were subsequently integrated into the development of a monitoring plan as discussed by Arts *et al.* (2011). Simulations using the ECLIPSE 100 black-oil simulator (*Schlumberger*, 2007) as undertaken by Nielsen *et al.* (2013) demonstrated that regional pressure propagation resulting from CO_2 injection can be mitigated by formation fluid extraction and that the structural filling is also enhanced by the integrated pressure management concept. Within the scope of the present study, these simulations were extended to three different scenarios of CO_2 injection (3 Mt CO_2/year) into the Gassum Formation to serve as input for the coupled hydro-mechanical simulations:

1. CO_2 injection without any formation fluid extraction;
2. CO_2 injection with formation fluid extraction equal to about 66% of the injected CO_2 volume at reservoir conditions;
3. CO_2 injection with formation fluid extraction equal to about 100% of the injected CO_2 volume at reservoir conditions.

2.1 Model Parameterization and Initialization

The reservoir simulation model was implemented with 250 × 250 elements in horizontal and 19 elements in vertical direction. Grid size in horizontal direction was maintained constant at 200 m × 200 m in the entire domain. Model initialization proceeded at hydrostatic pressure conditions derived from *in situ* measurements carried out in the Vedsted-1 well (*Tab. 1*). The vertical

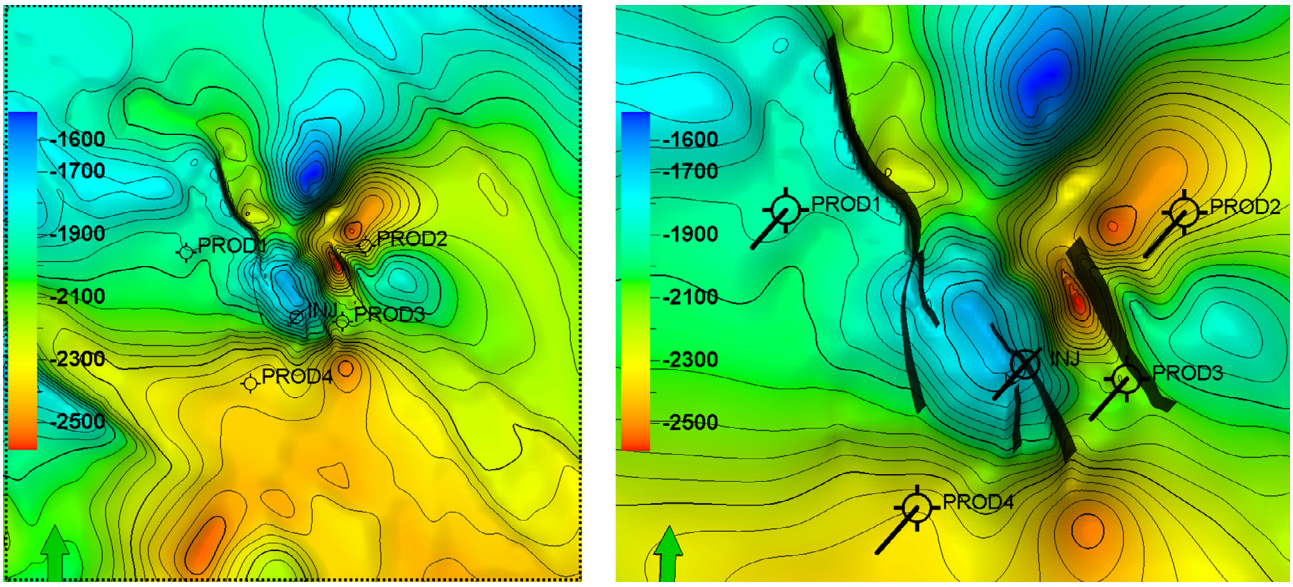

Figure 3

Plane (left) and rotated side views (right) of the main storage reservoir top (Gassum Formation top) with elevation depth (m TVD) including the proposed injection and extraction well locations and five major faults. Distance between the formation fluid extraction wells PROD1 and PROD3 is about 15 km and the dashed outline in the left figure represents the lateral size of the reservoir model with 50 km × 50 km (green arrow points into North direction).

TABLE 1

Densities and pore pressures used to calculate the vertical stress as input data for the numerical simulations derived from the Vedsted-1 well (Vattenfall, 2012, pers. comm.)

Lithological unit	Depth (m)	Density (kg/m^3)	S_v (MPa)	P_p (MPa)
Post Chalk Group	0	1 900	0.00	0.00
Chalk Group	37	2 112	0.69	0.37
Vedsted Formation	445	2 228	9.14	4.45
Frederikshavn Formation	850	2 186	18.0	8.51
Boerglum Formation	1 075	2 329	22.8	10.8
Haldager Formation	1 150	2 215	24.5	11.6
Fjerritslev Formation	1 240	2 362	26.5	12.5
Gassum Formation	1 825	2 298	40.0	18.8
Skagerrak Formation	2 138	2 415	47.1	22.2
Model basement	>5 000	2 700		

permeability distribution and vertical grid discretization applied in the reservoir model are plotted in Figure 1, whereby homogeneous permeability distributions were assigned to all layers without any lateral permeability variation. Furthermore, all five major faults were considered to be hydraulically conductive in lateral direction, since the average fault throw does exceed the formation thickness only at a few locations at depth of the Gassum Formation. The one well injector and four-well producer pattern was chosen to duplicate a scenario with four geothermal plants as discussed by Nielsen *et al.* (2013), where a net formation fluid extraction was simulated to investigate potential synergy effects of CO_2 storage combined with geothermal heat recovery. The individual

extraction well locations were determined by the location of four minor cities and municipalities. The ECLIPSE well option was applied for well control at all five wells and a pore volume multiplier of 1 000 was used to implement Dirichlet boundary conditions at the lateral model boundaries, whereas Neumann "no flow" boundary conditions were maintained at the model top and bottom.

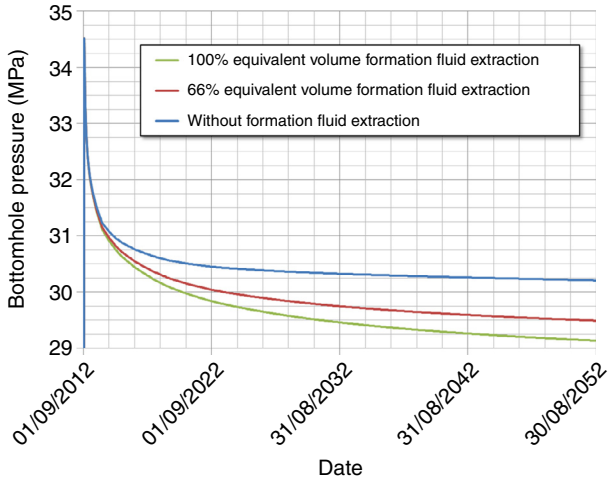

Figure 4

Simulated bottomhole pressures at the CO_2 injection well for the three injection and fluid extraction scenarios.

2.2 Simulation Results and Discussion

Figure 4 illustrates the development of bottomhole pressure at the injection well for the three investigated scenarios for a simulation time of 40 years (year 2012 to 2052). The maximum injection pressure at the start of injection operation does not exceed 35 MPa in all scenarios, whereas about 1.1 MPa difference are observed at the end of the injection operation between the 0% and 100% equivalent formation fluid extraction scenarios.

Figure 5 plots the differential pressure between initial conditions and a simulation time of 40 years. As expected, spatial pressure perturbation is significantly decreasing when formation fluid extraction from four extraction wells is carried out during CO_2 injection. Not taking fluid extraction into account leads to a pressure elevation of >1 MPa for a radius of up about 7.8 km around the injection well. This distance is reduced to a maximum radius of 4.6 km for the 66%

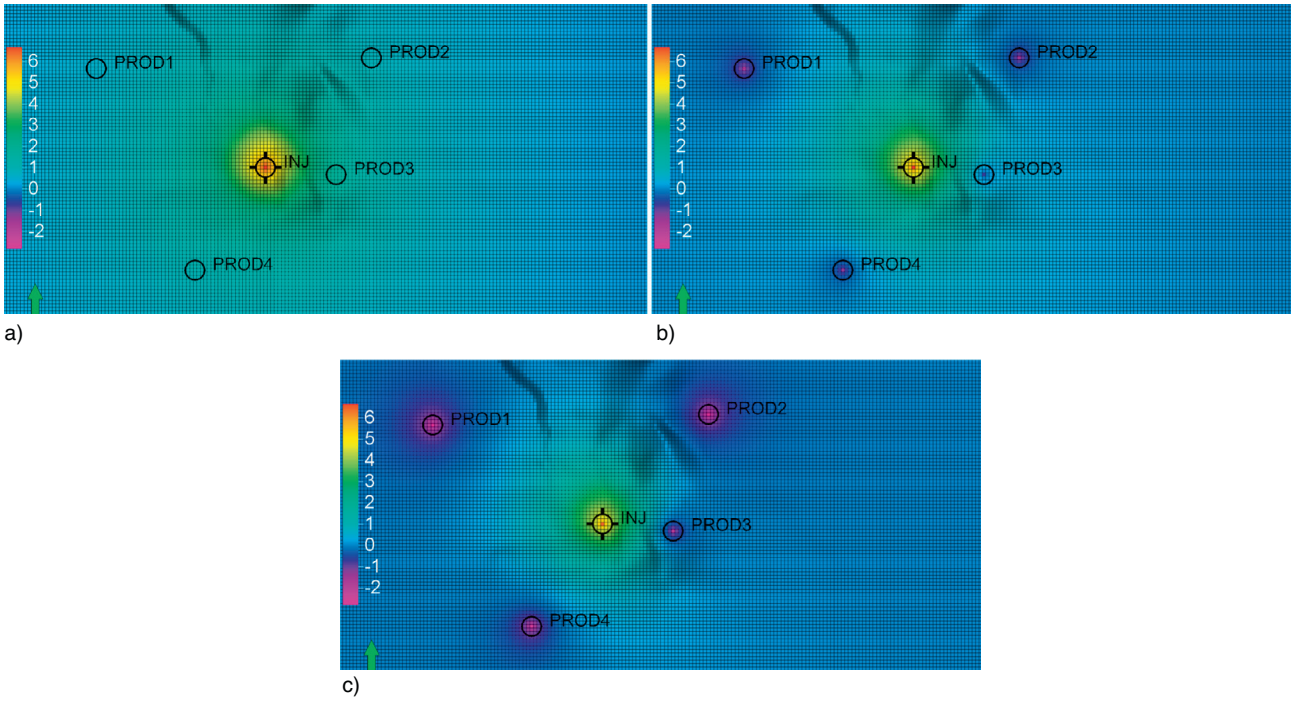

Figure 5

Differential pressure (Δp in MPa) for the three investigated CO_2 injection and formation fluid extraction scenarios: a) scenario without fluid extraction, b) 66% equivalent formation fluid extraction and c) 100% equivalent fluid extraction after 40 years of operation. The grid elements have a size of 200 m × 200 m and the distance between the fluid extraction wells PROD1 and PROD3 is about 15 km (green arrow points into North direction).

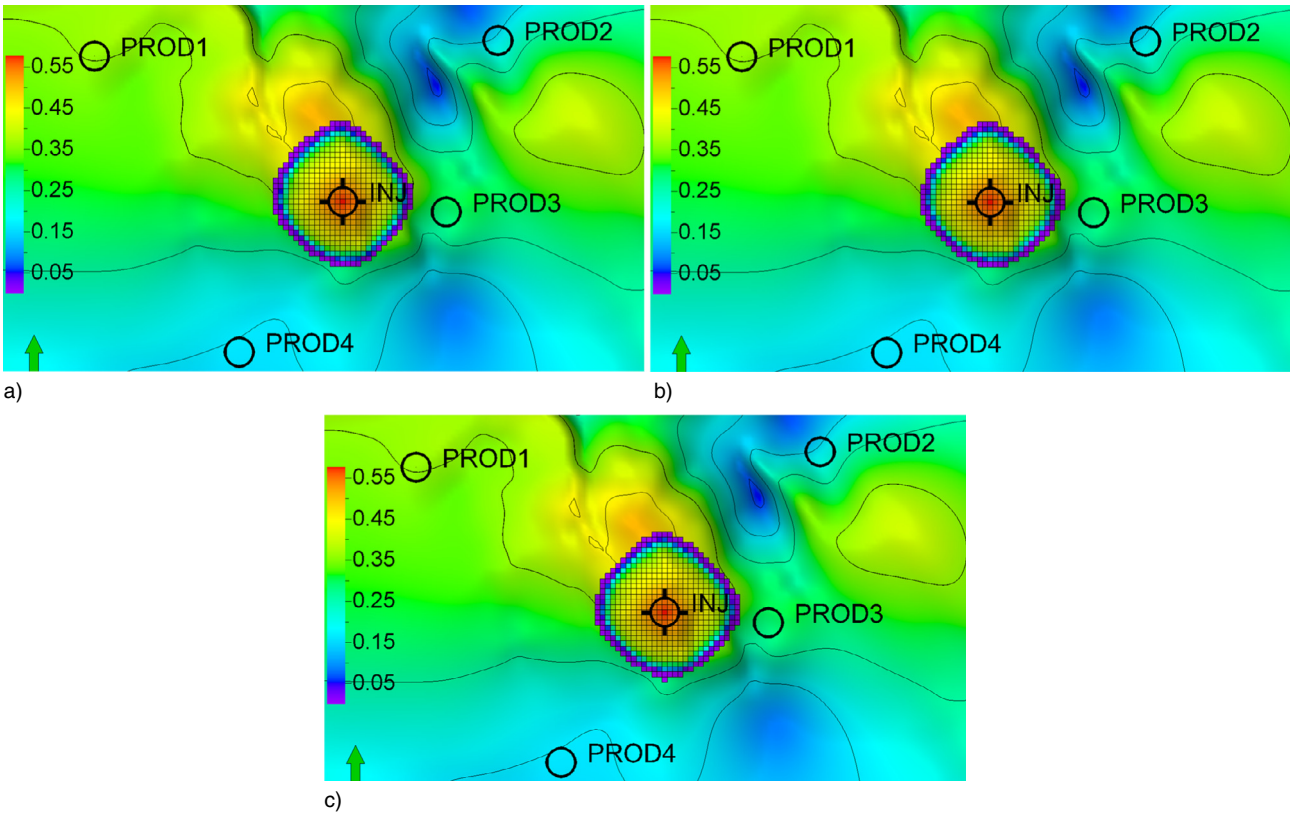

Figure 6

Spatial distribution of gaseous CO_2 saturation (–) after 40 years of injection (and fluid extraction in the Scenarios 2 and 3) for: a) no fluid extraction, b) 66% equivalent fluid extraction and c) 100% equivalent fluid extraction, using the four production wells. The distance between the fluid extraction wells PROD1 and PROD3 is about 15 km (green arrow points into North direction).

equivalent formation fluid extraction and to 3.9 km in the 100% equivalent formation fluid extraction scenarios. Thereby, a pressure decrease by more than 1 MPa in the vicinity of the extraction wells is only observed at a radius of about 150 m. As a maximum pressure decrease of 2.8 MPa is encountered in the vicinity of the formation fluid extraction wells for the 100% equivalent fluid extraction scenario, it is important to verify the potential geomechanical impacts of the proposed operation mode.

Hence, formation fluid extraction could also affect mechanical system integrity, especially when structural weakness zones as *e.g.* faults are located in close vicinity to the proposed wells.

Figure 6 demonstrates that fluid extraction increases the spatial CO_2 distribution, and thus enhances the pore space utilization as documented by Nielsen et al. (2013). The CO_2 plume shows a preferential migration in direction of the formation fluid extraction well PROD3 with increasing extraction rates, since this is the closest well to the CO_2 injector and all four wells produce at the same rate.

3 HYDRO-MECHANICAL SIMULATIONS

3.1 Numerical Model Geometry and Boundary Conditions

Using the regional 3D structural geological model, a 100 km × 100 km × 5 km geomechanical simulation model was developed comprising ten lithological units and five discrete faults (*Fig. 7*).

Figure 8 illustrates the numerical grid discretization applied for the hydro-mechanical simulation model. The inner model area close to all injection and extraction wells (22 km × 25 km) is discretized by 200 m × 200 m in the horizontal directions, whereas the vertical element size varies in the entire model depending on

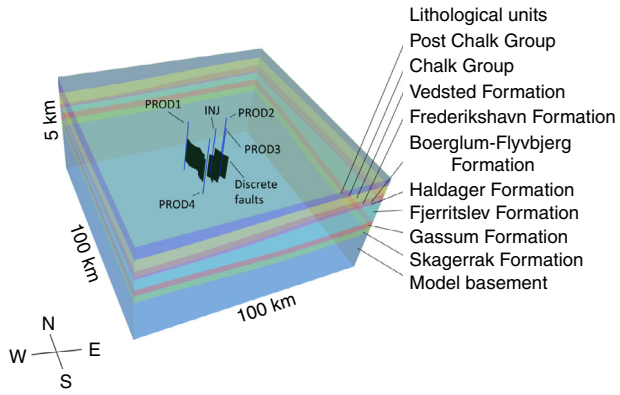

Figure 7

Lithological units as well as discrete faults and well locations implemented in the numerical hydro-mechanical model. Vertical exaggeration factor is 10.

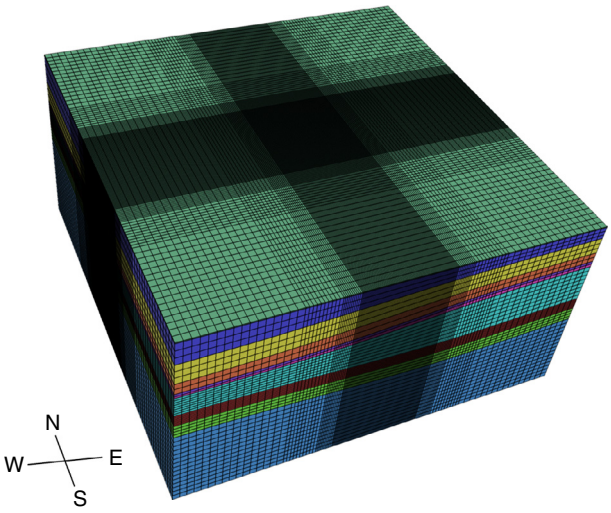

Figure 8

Numerical model grid with of 1 640 912 elements and refined horizontal discretization in the inner area close to the five wells (grid size 200 m × 200 m). Vertical exaggeration factor is 10.

the topography of the lithological units and is about 40 m at the depth of the CO_2 storage formation with a maximum of about 200 m. Lateral element size of the grid becomes coarser with decreasing distance to the model boundary, whereby a maximum horizontal element size of 1 600 m × 1 600 m is applied. The numerical model has a total of 1 640 912 elements with 182 × 196 × 46 elements in the *x*-, *y*- and *z*-direction, respectively. Thereby, 4 943 elements were implemented as FLAC3D ubiquitous joints elements introducing a weakness plane in each of these elements with a dip direction and angle assigned according to the respective fault. Zero displacement conditions were applied in normal direction at the bottom and lateral boundaries, while displacements are allowed at the top boundary.

A stress regime analysis carried out using regional data of the world stress map (Heidbach *et al.*, 2008) led to the assumption that the regional azimuth of the maximum horizontal stress S_{Hmax} is about 80° at the relevant depths derived from the closest known data from the Aars-1 well (situated about 38 km to the south of the Vedsted site) at 2 200 m depth. Two Leak Off Tests (LOT) carried out in the Thisted-4 well (situated about 60 km to the west of the Vedsted site) in the Chalk Group and the Haldager Sand Formation were used to derive the minimum horizontal stress S_{hmin} given with $S_{hmin} = 0.85\ S_v$, whereas S_v is the vertical stress determined by the gravitational load of the overburden. Using a stress polygon analysis as discussed by Moos and Zoback (1990) based on Anderson's (1951) faulting theory allowed us to determine the range of potential stress regimes from the given data. The stress regime at the Vedsted site can vary between a normal faulting ($S_v > S_{Hmax} > S_{hmin} = 0.85\ S_v$) and a strike-slip faulting regime ($S_{Hmax} > S_v > S_{hmin} = 0.85\ S_v$). Thereby, values of S_{Hmax} in the range of $0.85\ S_v < S_{Hmax} < 1.65\ S_v$ represent the bandwidth of maximum horizontal stresses (S_{Hmax}) given the previously mentioned assumptions (*Fig. 9*).

3.2 Model Parameterization and Initial Stress Regime Assessment

Density of the lithological units was derived from sonic logs measured in the Vedsted-1 well in addition to pore pressure (P_p) measurements that allow for calculation of vertical stress and pore pressure gradients for numerical model parameterization (*Tab. 1*).

Geomechanical properties are not available for the Vedsted site or at any structure close by. Literature data applied in the hydro-mechanical model is compiled in Table 2, whereby the dilation angle was assumed to be 0° for all lithological units. The model basement was parameterized with a high elastic modulus and low Poisson's ratio to provide a stable basis for the hydro-mechanical model. Fault properties were derived from Ouellet *et al.* (2010) and Nagelhout and Roest (1997) and implemented using the FLAC3D ubiquitous joint model (Itasca, 2012) with a joint cohesion of 0 MPa, a joint friction angle of 20° and dilation angle of 10° to maintain conservative assumptions but not

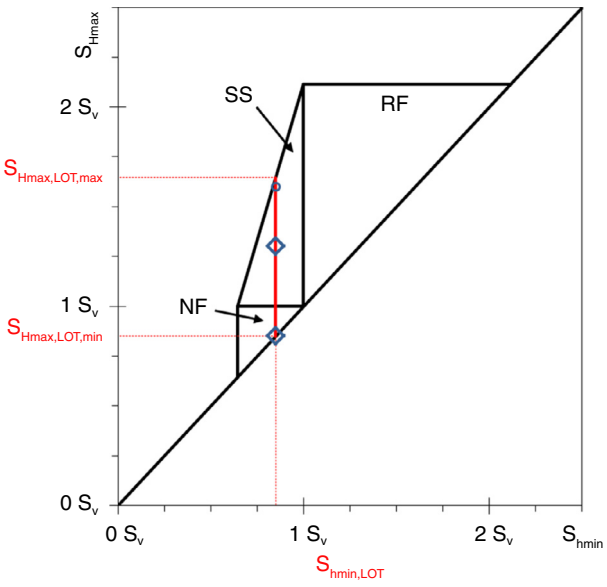

Figure 9

Stress polygon adapted for the Vedsted site based on leak-off tests and available well logs (faulting regimes are: NF - Normal Faulting, SS - Strike-Slip faulting, RF - Reverse Faulting). The blue rectangles indicate stress states considered in the hydro-mechanical simulations, while the stress state marked with blue circle was only assessed as potential initial stress state in the hydro-mechanical simulations. The solid red line represents the range of maximum horizontal stress (S_{Hmax}) that may be present at the Vedsted site based on LOT data.

underestimate potential shear and tensile failure. Dip direction and dip angle of the faults were assigned element-wise to the ubiquitous joint elements according to the fault geometry and the FLAC3D Mohr-Coulomb model was applied to the rock matrix. The FLAC3D ubiquitous joint model incorporates a weak-plane with a defined joint dip angle and direction into a model element which is cut by a fracture or fault. In the numerical computation, the Mohr-Coulomb failure criterion is applied for the element featuring the weak-plane after the rock matrix in that element has been assessed for failure. If failure in the rock matrix occurs, the stress state for that element is recalculated and the updated stress state then applied for weak-plane failure assessment (shear or tensile failure).

Figure 10 shows the stress state at the 4 943 elements of the five major faults for the four different stress regimes assessed by a numerical simulation carried out using the equilibrated mechanical model without changing the initial pore pressures (*i.e.* no fluid injection or extraction takes place). Here, fault failure is observed for the $S_{Hmax} = 1.60\ S_v$ stress regime directly after initial model equilibrium before the start of site operation. However, fault failure is not observed for the initial stress states $S_{Hmax} = 0.85\ S_v$ and $S_{Hmax} = 1.30\ S_v$ at this time. Figure 11 plots the locations of active fault shear failure (red elements) above the Gassum Formation at the high stress state ($S_{Hmax} = 1.60\ S_v$). Since vertical shear failure would occur along the fault planes at the depth of the Gassum Formation (target reservoir) in the latter stress scenario, a sustainable operation of a

TABLE 2

Geomechanical properties adapted from Ouellet *et al.* (2010), Bell (1977) and Nagelhout and Roest (1997)

Lithological unit	Elastic modulus (GPa)	Poisson ratio (–)	Friction angle (°)	Cohesion (MPa)	Tensile limit (MPa)
Post Chalk Group	3.5	0.47	35	0.0	0.00
Chalk Group	13.2	0.32	30	5.0	2.35
Vedsted Formation	9.5	0.21	25	5.0	5.00
Frederikshavn Formation	10.0	0.35	25	5.0	5.00
Boerglum Formation	9.5	0.21	25	5.0	5.00
Haldager Formation	19.9	0.35	25	5.0	5.00
Fjerritslev Formation	19.9	0.21	25	5.0	5.00
Gassum Formation	19.9	0.35	25	5.0	5.00
Skagerrak Formation	24.9	0.22	24	5.0	8.30
Model Basement	60.0	0.19	30	5.0	5.00

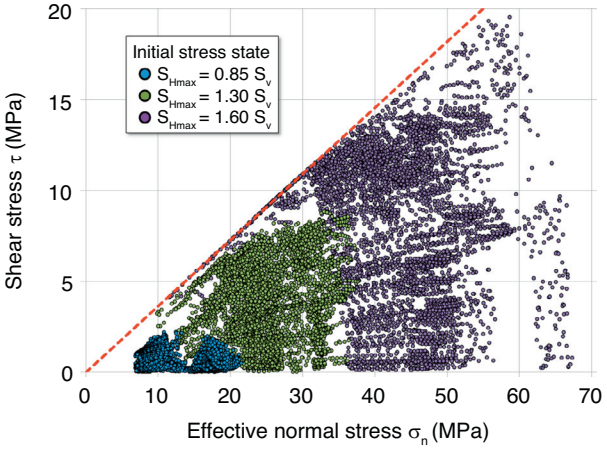

Figure 10

Effective normal *versus* shear stress plot for the fault elements in the assessed possible initial stress regimes at the Vedsted site. The $S_{Hmax} = 1.60\ S_v$ initial stress regime exhibits ubiquitous joints elements experiencing fault failure (located at the Coulomb failure line plotted as dashed red line).

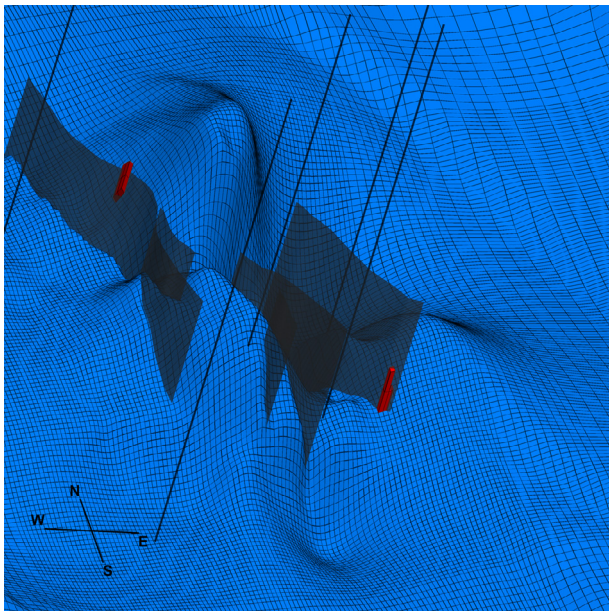

Figure 11

Fault shear failure (red elements) in the $S_{Hmax} = 1.60\ S_v$ initial stress regime. Blue topography represents the Gassum Formation top and transparent faces the five major faults. Lateral element size in the inner area is 200 m × 200 m.

CO_2 storage and synergetic geothermal heat recovery site would not be feasible at the Vedsted site, if the *in situ* stress state is given with $S_{Hmax} \geq 1.60\ S_v$. An active shear failure mechanism acting at a fault may generate pathways for fluid flow along that fault,

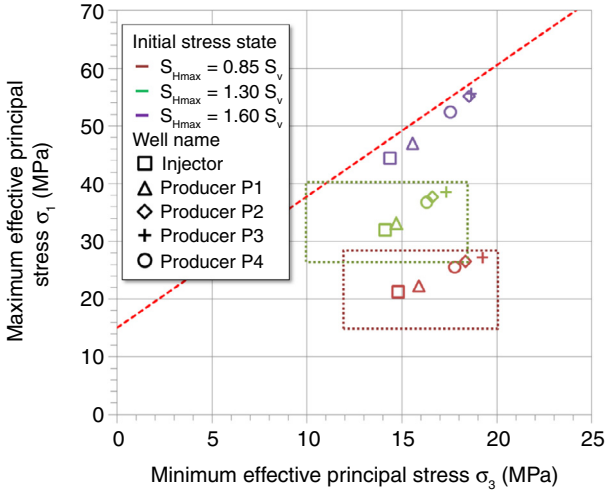

Figure 12

Initial stress states at the Gassum Formation top in the respective well blocks for the three assessed stress regimes. The dashed red line represents the Coulomb failure line. The dotted rectangles show the location of the detailed views of the investigated stress regimes ($S_{Hmax} = 0.85\ S_v$ and $S_{Hmax} = 1.30\ S_v$) plotted for all simulated time series in Figure 16.

and furthermore induce potential leakage of formation fluids into shallow freshwater aquifers (Tillner *et al.*, 2013b). Consequently, a comprehensive geomechanical exploration program is required to assess the *in situ* stress regime at the Vedsted site before starting the site operation. Well testing data gathered in the scope of such a site characterization program would allow for a more reliable assessment of the potential fault failure states supported by hydro-mechanical simulations.

Figure 12 illustrates the stress state at the injection and extraction wells at the initial model state. Since stress scenarios determined by $S_{Hmax} \geq 1.60\ S_v$ expose close to failure conditions at this time already, these scenarios were omitted in the further simulations. Thus, the $S_{Hmax} = 0.85\ S_v$ and $S_{Hmax} = 1.30\ S_v$ stress regimes were applied as initial conditions in the following coupled hydro-mechanical simulations to account for a potential stress regime variation in the given range ensuring that active faulting is not occurring at the Vedsted site to allow for the safe and reliable operation of CO_2 storage with simultaneous fluid extraction.

3.3 Simulation Results and Discussion

For the coupled hydro-mechanical simulations, two geomechanical models with different stress regimes (normal faulting and strike-slip faulting as discussed above) were

implemented and the geomechanical model subsequently equilibrated to represent the initial conditions according to the ratio of vertical to horizontal stresses at reservoir depth. Thereby, S_{Hmax}/S_v was implemented as initial stress condition with values of 0.85 for the normal faulting and 1.30 for the strike-slip faulting regime, while the other stress regimes discussed above were not further considered in the following numerical simulations. Both equilibrated hydro-mechanical models were then used as initial models for the subsequent simulations. Thereto, the spatial pore pressure distribution calculated in the reservoir simulations was upscaled from the 200 m × 200 m reservoir to the 200 m × 200 m (inner area) geomechanical simulation grid using the Petrel software package (*Schlumberger*, 2012) for three selected time steps of each scenario. This resulted in a total of nine mechanical equilibrium simulation runs for each stress regime, and thus in a total of 24 coupled hydro-mechanical simulation runs including the three initial equilibrium and initial failure state assessment simulations. The pore pressure distributions from the reservoir simulations were extracted at simulation times of 1 month (maximum pressure increase at the injection well), 20 years (intermediate CO_2 migration and pressure perturbation in the reservoir) and 40 years (end of injection and extraction cycle).

3.4 Vertical Displacements at the Storage Reservoir Top and Ground Surface

Figure 13 shows the vertical displacements at the ground surface and Gassum Formation top for the three injection and extraction scenarios at simulation times of 1 month, 20 years and 40 years. In the simulations carried out within the scope of the present study, the vertical displacements are almost identical for the normal and strike-slip faulting regimes, and thus not distinguished in the following. The initial vertical displacement calculated for the maximum bottomhole pressure after the first month of injection is about 0.5 mm for all scenarios, as the reservoir fluid extraction impact radius is not yet affecting the injection process. In the scenario without any fluid extraction from the storage formation, the calculated maximum vertical displacement at the reservoir top is 0.146 m after 20 years and 0.155 m after 40 years

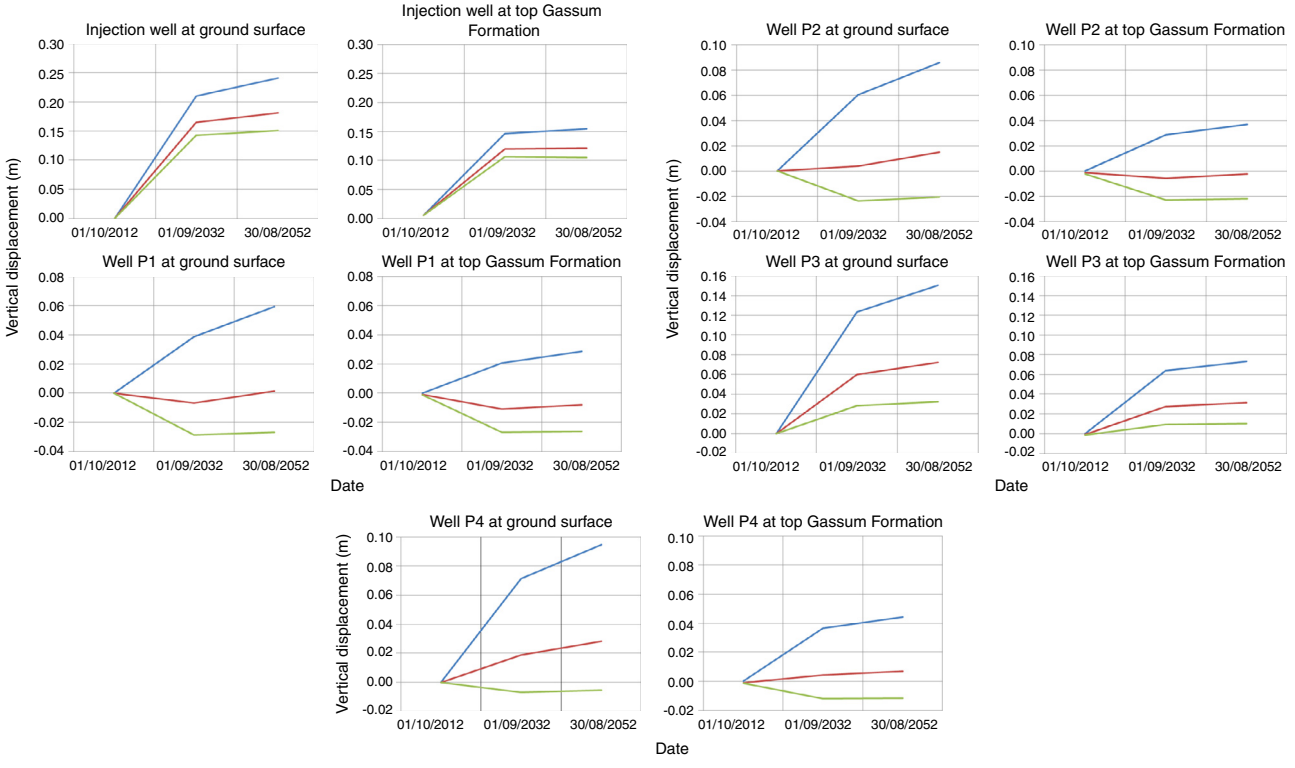

Figure 13

Development of vertical displacements (m) at the ground surface and Gassum Formation top for the no fluid extraction (blue line), the 66% equivalent fluid extraction (red line) and the 100% equivalent fluid extraction scenarios (green line).

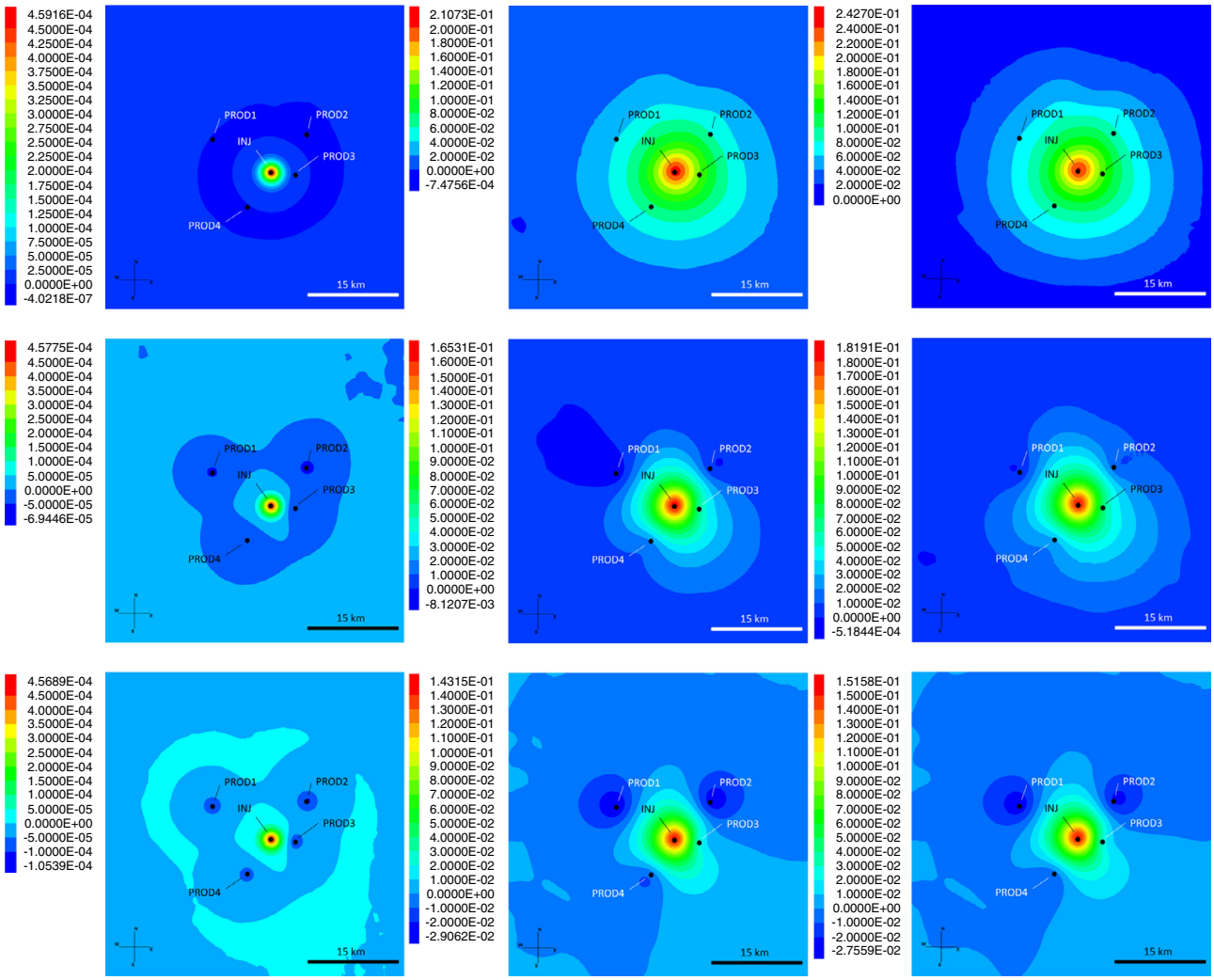

Figure 14

Comparison of vertical displacements (m) at the ground surface after 1 month (left), 20 years (middle) and 40 years (right) of simulation for the no fluid extraction (first row), the 66% equivalent fluid extraction (second row) and the 100% equivalent fluid extraction scenarios (third row).

of CO_2 injection. The 66% equivalent formation fluid extraction using four wells allows for a reduction of maximum vertical displacements by about 21% after 40 years of combined CO_2 injection and formation fluid extraction at the reservoir top. The 100% equivalent formation fluid extraction does achieve a vertical displacement mitigation of about 32% at the reservoir top. However, the extraction wells impact a maximum subsidence of 0.026 m at the reservoir top for the 100% equivalent extraction scenario that has to be considered in the ground movement assessment in the following.

Furthermore, Figure 13 exhibits that fluid extraction rates may be adapted to mitigate ground surface displacements during the entire time of site operation. Hereby, a specific adjustment of fluid extraction rates can support maintaining zero vertical displacements in the vicinity of the four formation fluid extraction wells. This is of special relevance for the present study, since the proposed extraction wells would be located close to urban infrastructure in the four selected cities and municipalities.

In addition to the development of vertical displacements (*Fig. 13*), Figure 14 illustrates the calculated spatial ground surface displacements in the study area at all simulation time steps. Surface uplift (and subsidence in the fluid extraction scenarios) is negligible for all scenarios at the first month of operation. The scenario without reservoir

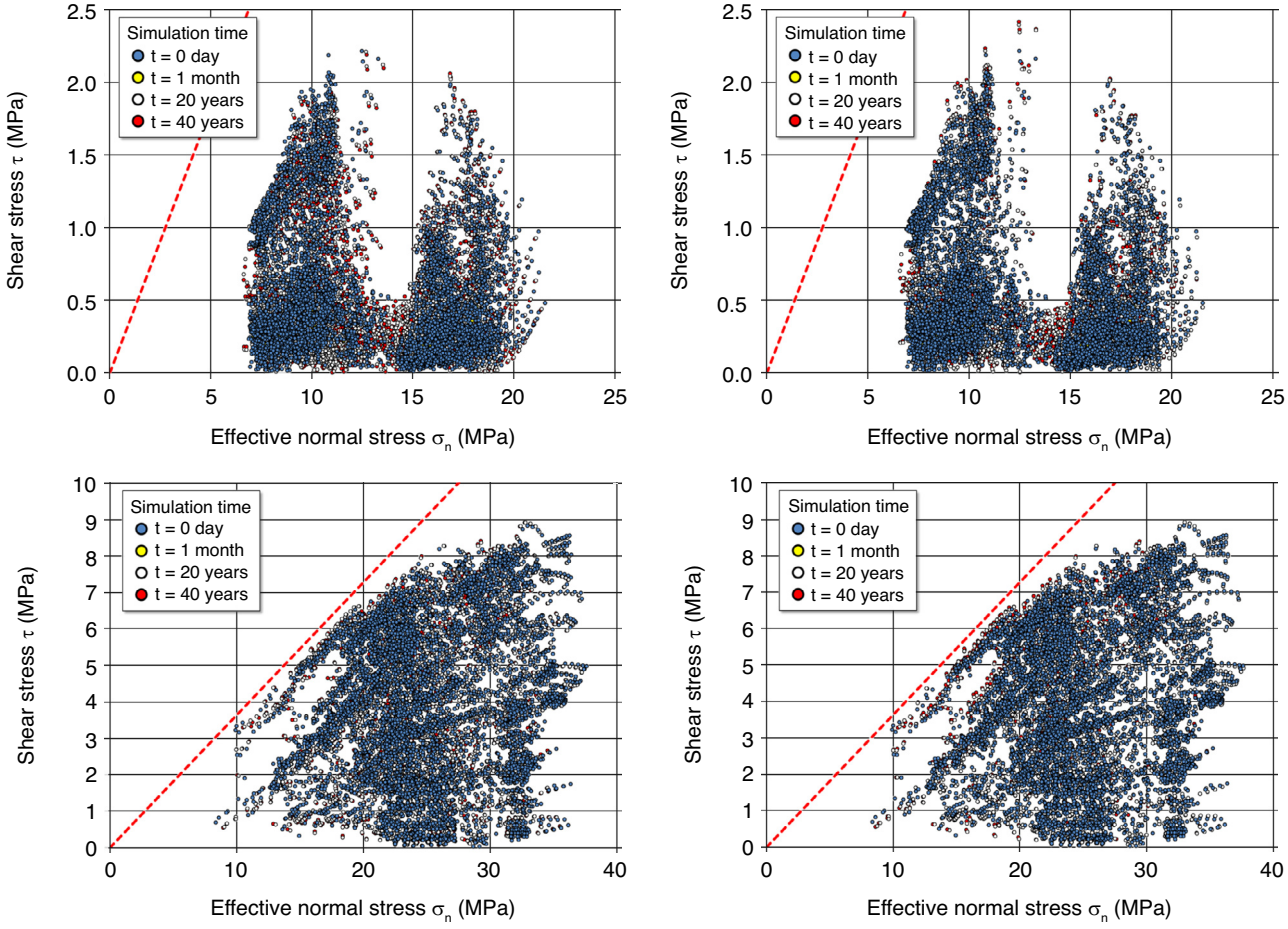

Figure 15

Effective normal *versus* shear stress plots including the cohesionless Coulomb failure line (dashed red line) for all 4 943 fault elements present in the mechanical model. Fault failure does not occur for the investigated stress regimes: S_{Hmax} = 0.85 S_v without any fluid extraction (top left) and 100% equivalent fluid extraction (top right) as well as S_{Hmax} = 1.30 S_v without any fluid extraction (bottom left) and 100% equivalent fluid extraction (bottom right).

management reveals a notable maximum ground uplift of 0.212 m after 20 years and 0.244 m after 40 years of CO_2 injection. The total areal impact of vertical displacements at the ground surface for this scenario amounts to a radius of about 20 km. Integration of pressure management allows for a mitigation of ground uplift in the 66% equivalent formation fluid extraction scenario, whereas a maximum surface uplift reduction by 22.0% after 20 years and by 24.8% after 40 years of simultaneous injection and extraction is achieved. In addition to that, the areal size of ground uplift can be significantly decreased depending on the location of the extraction wells. The 100% equivalent formation fluid extraction scenario shows a ground uplift reduction by 31.7% (after 20 years) to 37.3% after 40 years of simultaneous CO_2 injection and formation fluid extraction. However, it has to be considered that fluid extraction at the flow rates applied also induces ground subsidence of almost 0.03 m (extraction well PROD1, *Fig. 13*) after 20 years of injection resulting in a less homogeneous radial ground movement distribution around the injection well. Nevertheless, the areal size of ground surface displacements is again significantly reduced to a radius of less than 10 km.

3.5 Effective Stress and Failure Assessment

Unlike for vertical displacements, a differentiation between the investigated normal and strike-slip faulting regime has to be considered when addressing effective stresses as well as rock matrix and fault failure. For both investigated scenarios, all effective stress states experienced at the 4 943 fault elements (ubiquitous joints) in the three injection and extraction scenarios are in a safe distance to the cohesionless Coulomb failure line independent of

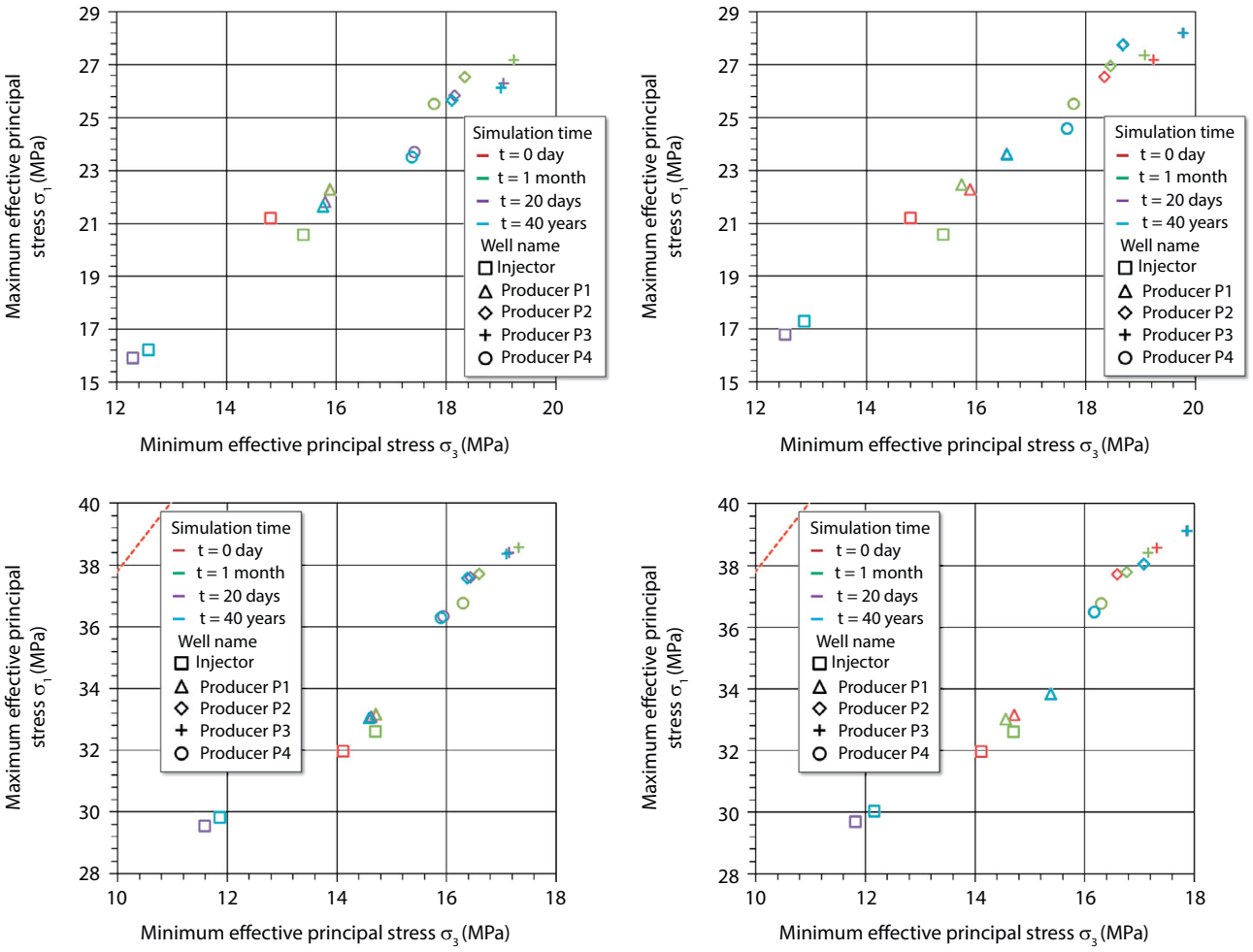

Figure 16

Stress state development at the five wells during site operation for the $S_{Hmax} = 0.85\ S_v$ scenarios without fluid extraction (top left) and with 100% equivalent volume fluid extraction (top right) as well as the $S_{Hmax} = 1.30\ S_v$ scenarios without fluid extraction (bottom left) and with 100% equivalent volume fluid extraction (bottom right). The dashed red line represents the Coulomb failure line.

the effective matrix cohesion (*Fig. 15*). For all investigated initial stress regimes and equivalent formation fluid extraction scenarios, stress paths at the fault elements are not notably changing at any time of operation. Furthermore, a sufficient distance to the Coulomb failure line is maintained indicating the absence of potential fault reactivation at the updated stress states.

The stress state development at the injection and extraction wells for the investigated $S_{Hmax} = 0.85\ S_v$ and $S_{Hmax} = 1.30\ S_v$ initial stress regimes is plotted in Figure 16 (magnification of the dotted rectangles in *Fig. 12*). For both stress regimes assessed, stress changes are significant especially at the injection well. However, a safe distance is maintained to the Coulomb failure line and tensile effective stresses do not occur at any time of simulation.

The hydro-mechanical simulations carried out in the scope of the present study demonstrate that whether fault nor rock matrix failure do occur at the selected operational modes independent of applied fluid injection and extraction regimes. Initial stresses between $S_{Hmax} = 0.85\ S_v$ (normal faulting stress regime) and $S_{Hmax} = 1.30\ S_v$ (strike-slip faulting regime) at the Vedsted site can be considered to allow for a safe operation of the proposed simultaneous CO_2 injection and equivalent formation fluid extraction scheme.

CONCLUSIONS

In the present study, the synergetic impact of simultaneous CO_2 injection and formation fluid extraction

was assessed from the hydro-mechanical point of view. Thereto, we carried out dynamic flow simulations of three different pressure management scenarios at the regional scale of a prospective CO_2 storage site located in northern Denmark. These three pressure management scenarios comprised CO_2 storage without formation fluid extraction as well as CO_2 storage with 66% and 100% equivalent volume formation fluid extraction. The dynamic flow simulation results show that a total pressure decrease of up to about 1.1 MPa at the injection well may be achieved at the end of CO_2 injection (100% equivalent volume extraction), that the sweep efficiency of the CO_2 can be increased by a spatial CO_2 plume extension as a result of formation fluid extraction, and that the areal pressure perturbation can be significantly decreased.

Based on a stress analysis carried out for the study area, two different stress regimes were considered in the coupled hydro-mechanical simulations. Supported by Leak Off Test (LOT) data, we identified that potential stress regimes in the study area may range from normal to strike-slip faulting with magnitudes of $S_{Hmax} = 0.85\ S_V$ (normal faulting stress regime) to $S_{Hmax} < 1.65\ Sv$ (strike-slip faulting stress regime). The three implemented hydro-mechanical models were calibrated to three different initial stress regimes ($S_{Hmax} = 0.85\ S_V$, $S_{Hmax} = 1.30\ S_V$ and $S_{Hmax} = 1.60\ S_V$) and then run until a mechanical equilibrium was achieved. Since stress regimes $S_{Hmax} \geq 1.60\ S_V$ imply active fault shear failure at two major faults at the Vedsted site already at the initial stress state, these stress regimes were omitted in the further hydro-mechanical integrity assessment. Active faulting regimes do generally not allow for a safe operation of a combined CO_2 storage and geothermal heat recovery site, so that the proposed operations would not be carried out in the presence of two active major regional faults. Consequently, two stress regimes ($S_{Hmax} = 0.85\ S_V$ and $S_{Hmax} = 1.30\ S_V$) were considered in the coupled hydro-mechanical simulations resulting in one initial equilibration run for each regime including three time step simulations for each of the three pressure management scenarios, and hence 24 coupled hydro-mechanical simulation runs in total involving the equilibration runs and verification of absence of initial rock matrix and fault failure without any fluid injection and extraction. The results show a maximum ground surface uplift of 0.24 m for the simulations without fluid extraction and ground uplift mitigation potential of 22.0% to 37.3% depending on the applied formation fluid extraction rates in the simulated pressure management scenarios. The simulation results show that fluid extraction rates may be adapted to mitigate ground surface displacement during the entire time of site operation. Thereby, a proper adjustment of fluid extraction rates can allow for maintaining zero vertical displacements in the vicinity of the four fluid extraction wells. This is especially relevant for the selected study area, since the proposed extraction wells would be located close to urban infrastructure in the four selected cities and municipalities where displacement mitigation is one requirement for a successful realization of the proposed operation mode.

Neither rock matrix nor fault failure do occur at the assessed stress regimes in all investigated scenarios, as the initially safe distance to the Coulomb failure line is maintained at any time of site operation. Initial stresses between $S_{Hmax} = 0.85\ S_v$ (normal faulting stress regime) and $S_{Hmax} = 1.30\ S_v$ (strike-slip faulting regime) at the Vedsted site can be considered to support a safe operation of the proposed simultaneous CO_2 injection and equivalent formation fluid extraction operation.

In order to improve the reliability of the simulation results, it is necessary to carry out a sufficient amount of leak of injection tests in the proposed new wells at the prospective study area combined with borehole and sonic logs to derive the azimuth of maximum horizontal stresses and stress magnitude development over depth. Furthermore, geomechanical testing of core samples would enable us to integrate more reliable data on the geomechanical properties into the numerical simulation models. From the numerical modeling perspective, FLAC3D allows to implement faults by interfaces featuring the calculation of shear displacements that can be then evaluated in dynamic flow simulations to assess the potential initial states and changes of fault aperture. Given these information, it would become possible to quantify potential fault leakage for CO_2 and formation fluids in the stress regime not considered due to the occurrence of active faulting at the initial stress state ($S_{Hmax} \geq 1.60\ S_V$). Thereto, a two-way coupling between the hydro-mechanical and reservoir simulators using a dual permeability approach could be employed.

ACKNOWLEDGMENTS

The research leading to these results has received funding from the European Union Seventh Framework Programme (FP7/2007-2013) under grant agreement No. 256705 (SiteChar project) as well as from *Enel*, *Gassnova*, *PGNiG*, *Statoil*, *Vattenfall*, *Véolia Environnement*, and the Scottish Government. The authors are grateful for that support, and furthermore would like to thank the two anonymous reviewers for their constructive comments improving the manuscript quality.

REFERENCES

Anderson E.M. (1951) *Dynamics of Faulting and Dike Formation with Application in Britain*, 2nd ed., Oliver and Boyd, Edinburgh, 206 p.

Arts R.J., Jones D.G., Chadwick R.A., Klinkby L., Bernstone C., Sørensen A.T. (2011) Development of a monitoring plan for the Vedsted structure in Denmark, *Energy Procedia* **4**, 3558-3565.

Bell F.G. (1977) A note on the physical properties of chalk, *Engineering Geology* **11**, 217-225.

Bergmo P.E.S., Grimstad A.A., Lindeberg E. (2011) Simultaneous CO_2 injection and water production to optimize aquifer storage capacity, *International Journal of Greenhouse Gas Control* **5**, 555-564.

Britze P., Japsen P. (1991) Geological map of Denmark 1:400,000. The Danish Basin. "Top Zechstein" of the Triassic (two-way traveltime and depth, thickness and interval velocity). Geological Survey of Denmark Map Series 31. 4 maps and 4 pp.

Buscheck T.A., Sun Y., Chen M., Hao Y., Wolery T.J., Bourcier W.L., Tompson A.F. (2012) Active CO_2 reservoir management for carbon storage: Analysis of operational strategies to relieve pressure buildup and improve injectivity, *International Journal of Greenhouse Gas Control* **6**, 230-245.

Court B., Bandilla K.W., Celia M.A., Buscheck T.A., Nordbotten J.M., Dobossy M. (2012) Initial evaluation of advantageous synergies associated with simultaneous brine production and CO_2 geological sequestration, *International Journal of Greenhouse Gas Control* **8**, 90-100.

Dalhoff F., Klinkby L., Sørensen A.T., Bernstone C., Frykman P., Andersen C., Christensen N.P. (2011) CCS demo Denmark: The Vedsted case, *Energy Procedia* **4**, 4704-4710.

Frykman P., Bech N., Sørensen A.T., Nielsen L.H., Nielsen C. M., Kristensen L., Bidstrup T. (2009) Geological modeling and dynamic flow analysis as initial site investigation for large-scale CO_2 injection at the Vedsted structure, NW Denmark, *Energy Procedia* **1**, 1, 2975-2982.

Frykman P., Nielsen C.M., Dalhoff F., Sørensen A.T., Klinkby L., Nielsen L.H. (2011) Geological modelling for site evaluation at the Vedsted structure, NW Denmark, *Energy Procedia* **4**, 4711-4718.

Heidbach O., Tingay M., Barth A., Reinecker J., Kurfeß D., Müller B. (2008) The World Stress Map database release 2008. doi:10.1594/GFZ.WSM.Rel2008

Itasca (2012) FLAC3D – Fast Lagrangian Analysis of Continua in 3 Dimensions. User's Manual.

Klinkby L., Nielsen C.M., Krogh E., Smith I.E., Palm B., Bernstone C. (2011) Simulating rapidly fluctuating CO_2 flow into the Vedsted CO_2 pipeline, injection well and reservoir, *Energy Procedia* **4**, 4291-4298.

Larsen M., Bidstrup T., Dalhoff F. (2003) CO_2 storage potential of selected saline aquifers in Denmark. Danmarks og Grønlands Geologiske Undersøgelse Rapport 2003/39, 83 pp.

Magri F., Tillner E., Wang W., Watanabe N., Zimmermann G., Kempka T. (2013) 3D Hydro-mechanical Scenario Analysis to Evaluate Changes of the Recent Stress Field as a Result of Geological CO_2 Storage, *Energy Procedia* **4**, 375-383.

Moos D., Zoback. M.D. (1990) Utilization of observation of well bore failure to constrain the orientation and magnitude of crustal stresses: application to continental deep sea drilling project and ocean drilling program boreholes, *Journal of Geophysical Research* **95**, 9305-9325.

Nagelhout A.C.G., Roest J.P.A. (1997) Investigating fault slip in a model of an underground gas storage facility, *International Journal of Rock Mechanics and Mining Sciences* **34**, 3-4, Paper No. 212.

Nielsen L.H. (2003) Late Triassic – Jurassic development of the DanishBasin and the Fennoscandian Border Zone, southern Scandinavia, Ineson J.R., Surlyk F. (eds), The Jurassic of Denmark and Greenland, *Geological Survey of Denmark Bulletin* **38**, 459-526.

Nielsen C.M., Frykman P., Dalhoff F. (2013) Synergy Benefits in Combining CCS and Geothermal Energy Production, *Energy Procedia* **37**, 2622-2628.

Ouellet A., Bérard T., Frykman P., Welsh P., Minton J., Pamucku Y. (2010) Reservoir geomechanics case study of seal integrity under CO_2 storage conditions at Ketzin, Germany, *Ninth Annual Conference on Carbon Capture and Sequestration 2010*, 10-13 May.

Röhmann L., Tillner E., Magri F., Kühn M., Kempka T. (2013) Fault Reactivation and Ground Surface Uplift Assessment at a Prospective German CO_2 Storage Site, *Energy Procedia* **40**, 437-446.

Schlumberger (2012) Petrel Seismic-To-Evaluation Software, Version 2011.1, *Schlumberger* Information Solutions.

Schlumberger (2007) ECLIPSE 100, *Schlumberger* Information Solutions.

Tillner E., Kempka T., Nakaten B., Kühn M. (2013a) Geological CO_2 Storage Supports Geothermal Energy Exploitation: 3D Numerical Models Emphasize Feasibility of Synergetic Use, *Energy Procedia* **37**, 6604-6616.

Tillner E., Kempka T., Nakaten B., Kühn M. (2013b) Brine migration through fault zones: 3D numerical simulations for a prospective CO_2 storage site in Northeast Germany, *International Journal of Greenhouse Gas Control* **19**, 689-703.

Vidal-Gilbert S., Nauroy J.F., Brosse E. (2009) 3D geomechanical modelling for CO_2 geologic storage in the Dogger carbonates of the Paris Basin, *International Journal of Greenhouse Gas Control* **3**, 3, 288-299.

Manuscript accepted in May 2014
Published online in September 2014